PROCEEDINGS OF SPIE

SPIEDigitalLibrary.org/conference-proceedings-of-spie

Automated lineament extraction applied to high-resolution imagery Worldview-3 and LiDAR data for pegmatite mineral exploration

D. Santos, A. Mendes, A. Azzalini, J. Cardoso-Fernandes, A. Lima, et al.

D. Santos, A. Mendes, A. Azzalini, J. Cardoso-Fernandes, A. Lima, A. C. Teodoro, "Automated lineament extraction applied to high-resolution imagery Worldview-3 and LiDAR data for pegmatite mineral exploration," Proc. SPIE 12734, Earth Resources and Environmental Remote Sensing/GIS Applications XIV, 1273414 (19 October 2023); doi: 10.1117/12.2679367

SPIE.

Event: SPIE Remote Sensing, 2023, Amsterdam, Netherlands

Automated Lineament Extraction applied to high-resolution imagery Worldview-3 and LiDAR data for pegmatite mineral exploration

Santos, D.[1,2]*, Mendes, A.[1], Azzalini, A.[1], J. Cardoso-Fernandes[1,2], Lima, A.[1,2], Teodoro, A.C. [1,2]

[1]Institute of Earth Sciences, FCUP pole, Porto, Portugal; [2] Department of Geosciences, Environment and Spatial Planning Faculty of Sciences of the University of Porto, Portugal;

ABSTRACT

Lineament extraction is a commonly used technique in mineral exploration to identify geological structures such as fault scarps, joints, and folds. However, the accuracy of this technique can be limited by factors such as the low spatial resolution of the data. This study aims to address these limitations by exploring the potential of high spatial resolution data for extracting linear structures in Tysfjord, northern Norway. Two types of high-resolution data were utilized for lineament extraction: (i) WorldView-3 (WV3) satellite orbital imagery with a ground sample distance (GSD) of 2 meters, and (ii) Light Detection And Ranging (LiDAR) point cloud data, with a GSD of 1 meter. The LiDAR point cloud was utilized to generate a Digital Terrain Model (DTM), and automated lineament extraction was performed on both WV3 and LiDAR data using the lineament algorithm (LINE) available in PCI Geomatics software. A comparison was conducted using Sentinel 2 images to analyze the impact of utilizing high-resolution images on the final results. The outcomes illustrate that high-resolution images hold substantial potential for extracting lineaments and can aid in identifying mineral deposits and neotectonic activity. In the future, these findings could be integrated with other remote sensing methods to enhance the capabilities of remote sensing for mineral exploration.

Keywords: high spatial resolution; high-resolution images; mineral exploration; Tysfjord.

1. INTRODUCTION

Geological formations are crucial factors in determining the presence of mineral deposits and, at a regional level, these characteristics can be mapped using different spatial data sources[1]. It is possible to extract lineaments applying manual[2], automatic [3] or semiautomatic [4] lineament extraction methods, but in this work, just the automatic method was applied. The automatic lineament extraction has some advantages in relation to manual methods such as it is easier to run, it is faster, and it does not depend on the quality of the analysis and user experience[5–7]. The automatic lineament extraction is performed by analyzing digital images using computer-assisted software[8]. According to Dossary et al., [9] the content of the information present in the base image and process factors such as the noise, the threshold, the size, and the orientation of the linear features are crucial for the efficiency of the automatic extraction[10]. Considering these factors, it is clear the impact of the spatial resolution of the satellite images in this process. Previous studies[7] have evaluated the potential of DEM data for lineament extraction in Tysfjord, but high-resolution imagery was not used. This work aims to apply automatic lineament extraction in different data with different spatial resolutions, comparing their results, and analyzing the potential of high-resolution data to extract geological linear features in Tysfjord, Norway. Two very high spatial resolution data were processed: a Worldview 3 (band 7) image with 2 m of ground sample distance **(**GSD), and a LiDAR-derived Digital Terrain Model (DTM) hillshade with 1 m of GSD. Band 8 of Sentinel 2 also was used to compare the results with the very high-resolution data. The image processing was done through PCI Geomatics software(version 2018). After extraction, it was necessary to analyze the lineaments and delete the ones with no geological importance. After that, densities maps were composed to analyze the concentration of the lineaments

*douglas.santos@fc.up.pt

Earth Resources and Environmental Remote Sensing/GIS Applications XIV, edited by Karsten Schulz,
Ulrich Michel, Konstantinos G. Nikolakopoulos, Proc. of SPIE Vol. 12734, 1273414
 · doi: 10.1117/12.2679367

2. STUDY AREA

The Tysfjord region in northern Nordland, Norway, specifically the Tysfjord-Hamarøy pegmatite field (Figure 1), has a mining legacy spanning over a century. Initially focused on ceramic feldspar, since 1975, it shifted to extracting high-purity quartz, vital for high-tech products due to its low trace elements. The field comprises NYF-type pegmatite bodies within the Trans-Scandinavian Igneous Belt. Husdal's classification divides Tysfjord pegmatites into (i) metapegmatites and (ii) pegmatites based on age, size, and deformation. Müller et al. highlighted their enrichment in rare elements and defined two stages of pegmatite formation: (i) during Svecofennian, linked to tectonic-metamorphic events, and (i) Caledonian, marked by orogenic-metamorphic activity. The Svecofennian pegmatites derived from residual melts and underwent multiple deformation phases resulting in large-scale shearing of the pegmatite bodies, while the Caledonian pegmatites derived from partial melting of the Tysfjord granitic gneiss during late Caledonian events[11] . These younger pegmatites generally show a N-S strike parallel to inherited ancient Precambrian structures that were reactivated during the Caledonian orogeny and that could have served for pegmatite melt emplacement [12,13] . In the Tysfjord area, about 20 pegmatites were emplaced along several parallel or diverging structures in a 4 km long array which was presumably ductile during melt emplacement.

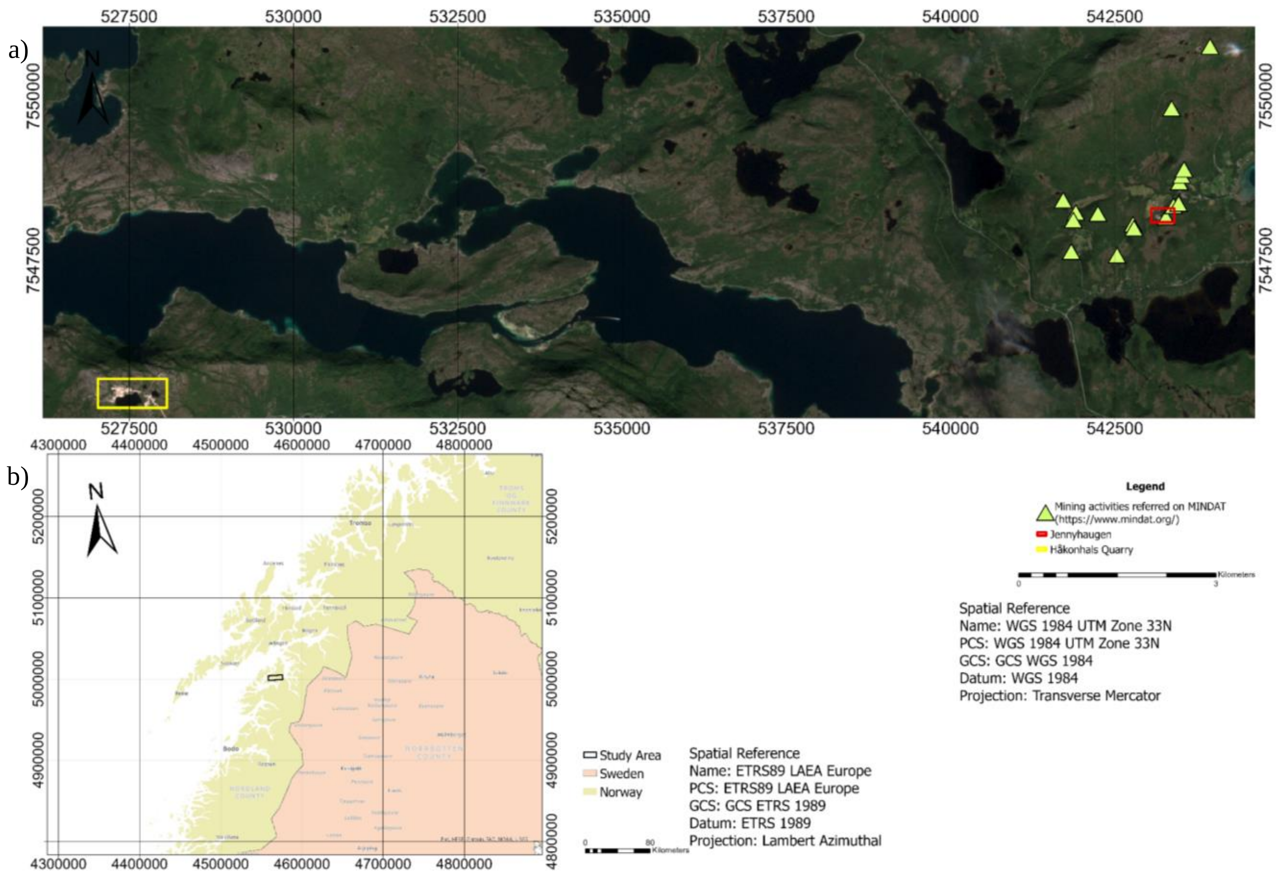

Figure 1. Study area location. The Hakonhals and Jennyhaugen mines are highlighted by the yellow and red rectangles respectively. a) An overview of the study area. b) Study area location in Europe.

3. METHODOLOGY

3.1 Data and preprocessing

The WV3 image was acquired on May 23, 2022. The image has eight bands in the VNIR region (with 2 meters of GSD), and eight bands in the SWIR region (with 3.7 meters of GSD). A panchromatic band is also provided with 0.5 meters of GSD. A DTM (Digital Terrain Model) was also acquired, provided by the Norwegian government (Hoydedata.no), and based on LiDAR technology. After the acquisition of the DTM, a hillshade was applied to the terrain topography to help to interpret the analyses of the results. A Sentinel 2 MSI image was acquired on September 28, 2019, and was used in this study as a baseline indicator to compare with the results obtained with high-resolution data. The atmospheric correction of the Sentinel 2 image was computed through Dark object subtraction (DOS1)[14].
The VNIR, SWIR, and panchromatic bands of WV3 images are provided in separate products. Consequently, before preprocessing the image, it was necessary to do a layer stacking to bring together the SWIR and VNIR bands into one dataset. To avoid many mosaics, the tiled images were chosen to compute the band stack. In the next step, the RPC Orthorectification Workflow available in ENVI software version 5.6.3[15] was used to perform an orthorectification, and the ATCOR Ground Reflectance (PCI Geomatica 2018) was applied to convert the Top Of Atmosphere (TOA) reflectance into surface reflectance. Two tiled images were necessary to cover the entire study area. One tiled image, in the west of the study area, encompasses the Hakonhals mine (A1), and the other one, in the east, encompasses the Jennyhaugen mine (A2). Nevertheless, after applying raze removal to minimize visible haze effects, it was possible to see that the raze removal negatively impacted the tiled image of A2. Thus, it was decided to keep the images separated. After preprocessing bands 7 (NEAR IR1) and 8 (NEAR IR) of the WV3 and Sentinel 2 respectively, were chosen as input for the automated lineament extraction processes.

3.2 Automated Lineament Extraction

As a crucial role in determining the formation deposits, the geological structures can be identified through various spatial data[16,17]. In this research, the focus will be on automatic lineament extraction. This method was chosen due to its reproducibility and efficiency regarding the final results[18–20]. In this study, the lineament was performed by the lineament extraction algorithm (LINE) available in PCI Geomatic software. The parameters chosen for each data can be observed in Table 1.

The **Filter Radius (RADI)** Specifies the radius (in pixels) to be used in the edge's detection filter, aiming to utilize lower values for detecting more intricate details and higher values to minimize noise detection. This parameter significantly influences the ability to detect small details in the processed image. The **Edge Gradient Threshold (GTHR)** defines the threshold of brightness change and represents the minimum gradient value required to be considered as an edge during the edge detection process. The **Length Threshold (LTHR)** expounds the minimum length of curve (in pixels) used for mapping curved linear objects, that are taken as the lineament for further consideration. The **Fitting Error Threshold (FTHR)** specifies the allowed tolerance when fitting an arc or line segment to form a curved lineament. Ideally, values between 2 and 5 are recommended. The **Angular Difference Threshold (ATHR)** is the parameter that defines the maximum angle (in degrees) that allows two neighboring polylines to be linked. And finally, the **Linking Distance Threshold (DTHR)** is a measurement that specifies the minimum distance (in pixels) required between the endpoints of a polyline to be linked. Recommended distance values range from 10 to 45 pixels[19,21].

Table 1. Parameters used in the lineament extraction algorithm.

	RADI	GTHR	LTHR	FATHER	ATHR	DTHR
WV3	10	100	30	3	30	20
DTM	5	100	30	3	30	20
Sentinel 2	10	100	30	3	30	20

3.3 Post-processing

Many of the lineaments extracted by automatic methods have no geological importance. Therefore, after the lineament extraction a post-processing control is necessary to discard those non-geological lineaments and other false positives such as roads, tracks, lakes, and cultivated areas, amongst others (e.g. coastal areas). These data were manually removed in a GIS environment[7] using a high-resolution true color map composition from the WV3 satellite.

4. RESULTS AND DISCUSSION

4.1 Lineament extraction

The lineament extraction results in 245 lineaments for Sentinel 2 (Figure 2 a), 1383 lineaments for WV3 (Figure 2 b), and 1974 lineaments for the DTM hillshade (Figure 2 c). By analyzing the results, it's possible to observe that the Sentinel 2 lineaments have a minimum length of 300 m and a maximum length of 2549 m. The WV3 lineaments have a minimum length of 60 m and a maximum length of 593 m. DTM lineaments have a minimum length of 30 m and a maximum length of 588 m (Figure 3). The results indicate that the lineament length is influenced by the spatial resolution of the data used as input in the lineament extraction. The higher the spatial resolution, the smaller the length of the lineaments. With a lower spatial resolution, it is more difficult to detect smaller structural details, which were detected on very high-resolution images. This can explain the increased number of extracted lineaments when we compare the Sentinel 2 (245), the WV3 (1383), and the DTM hillshade (1974). Analyzing the results by length, we observed that most abundance lineaments are between 30-50 m for DTM hillshade (52%), between 60-100 m for WV3 lineaments (62%), and between 400-600 m for Sentinel 2 (33%). The complete values of the relationship between the quantity and length of the lineaments can be seen in Figure 4.

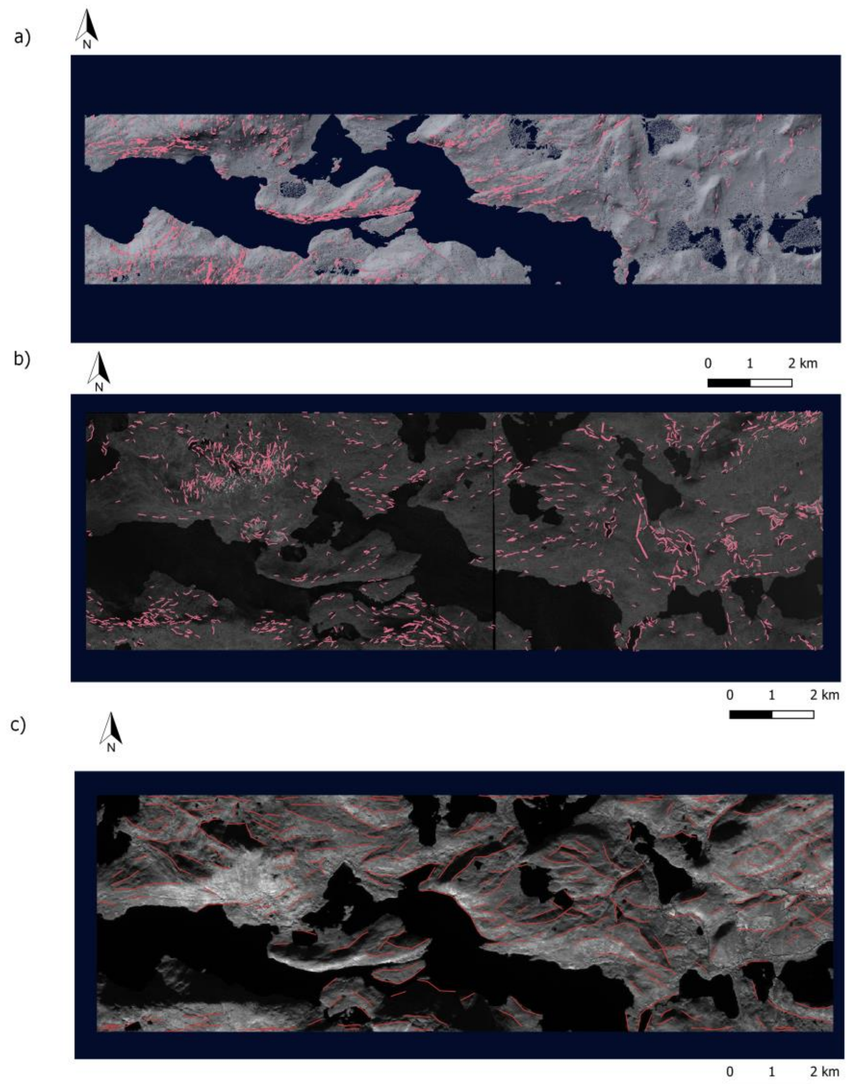

Figure 2. Automated lineament extraction results. The Lineaments are represented by red lines. a) Lineament extraction for DTM hillshade. b) Lineament extraction for WV3 image. c) Lineament extraction for Sentinel 2 image.

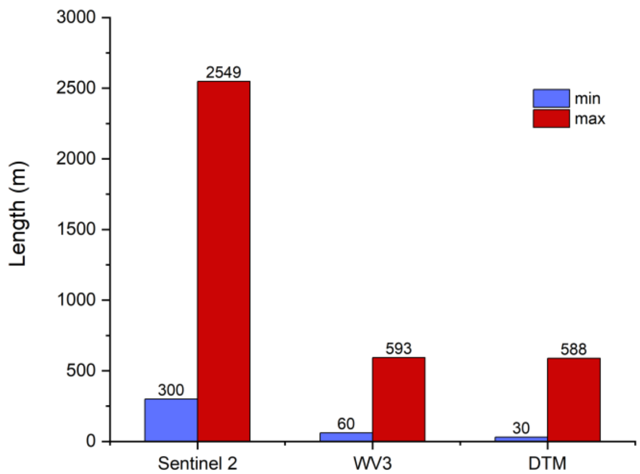

Figure 3 The minimum and maximum lengths of the extracted lineaments for each data type are represented in a bar graph.

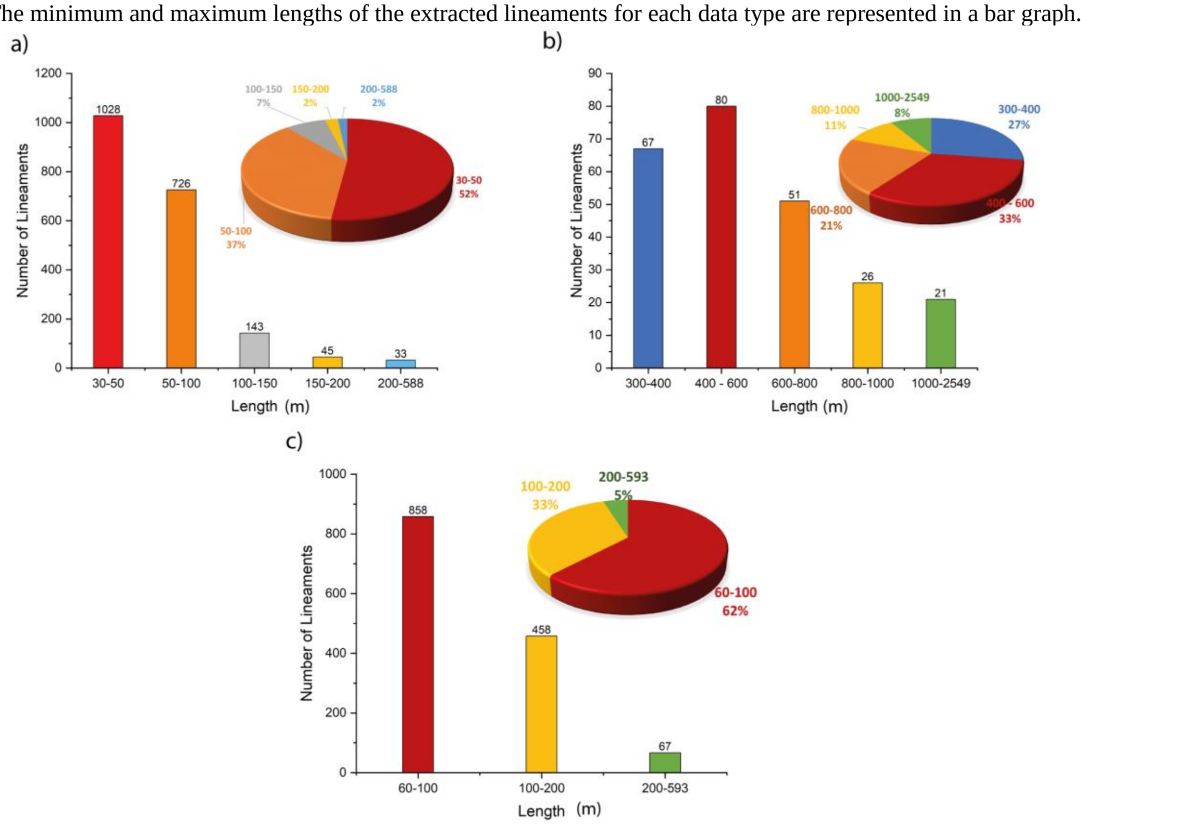

Figure 4. The number of lineaments according to the length and occupational percentage for the automatically extracted. a) DTM Hillshade. b) Sentinel 2 Band 8.. c) WV3 Band 7

4.2 Line density

The lineament density map allows us to do correlation analysis and provides us with information about the concentration of the lineaments per area[19,22]. In this research, a density map was made for each dataset of extracted lineament. The low concentration of the lineaments is represented in blueish colors and the high concentration is represented in red colour. The density for DTM hillshade lineaments shows some spots of high concentration in the west of the study area. Those high-density spots are around Finnøy island where are located the Hakonhals mine and Karlsøy quarry (Figure 5 a). The density map for WV3 lineaments (Figure 5 b) shows a high concentration around the Hakonhals mine and some spots of higher concentration 5 km northeast of the Hakonhals mine. We also observed some high density around Jennyhaugen mine at Drag, Hamarøy. The Sentinel 2 results indicate high-density zones around the Hakonhals mine and at the northeastern edge of the study area. Overall, the map displays an abundance of medium-density clusters (depicted in yellowish and orange colors) when utilizing the lower spatial resolution data. While the DTM density map (Figure 5 a) shows fewer medium-density clusters (in yellowish and orange colors), the Sentinel 2 density map (Figure 5 c) presents most of its lineaments in medium-density clustering. The density maps generated in this research will be integrated with classification processing methods results to form a robust analysis of the geological structures and outcrops at Tysfjord.

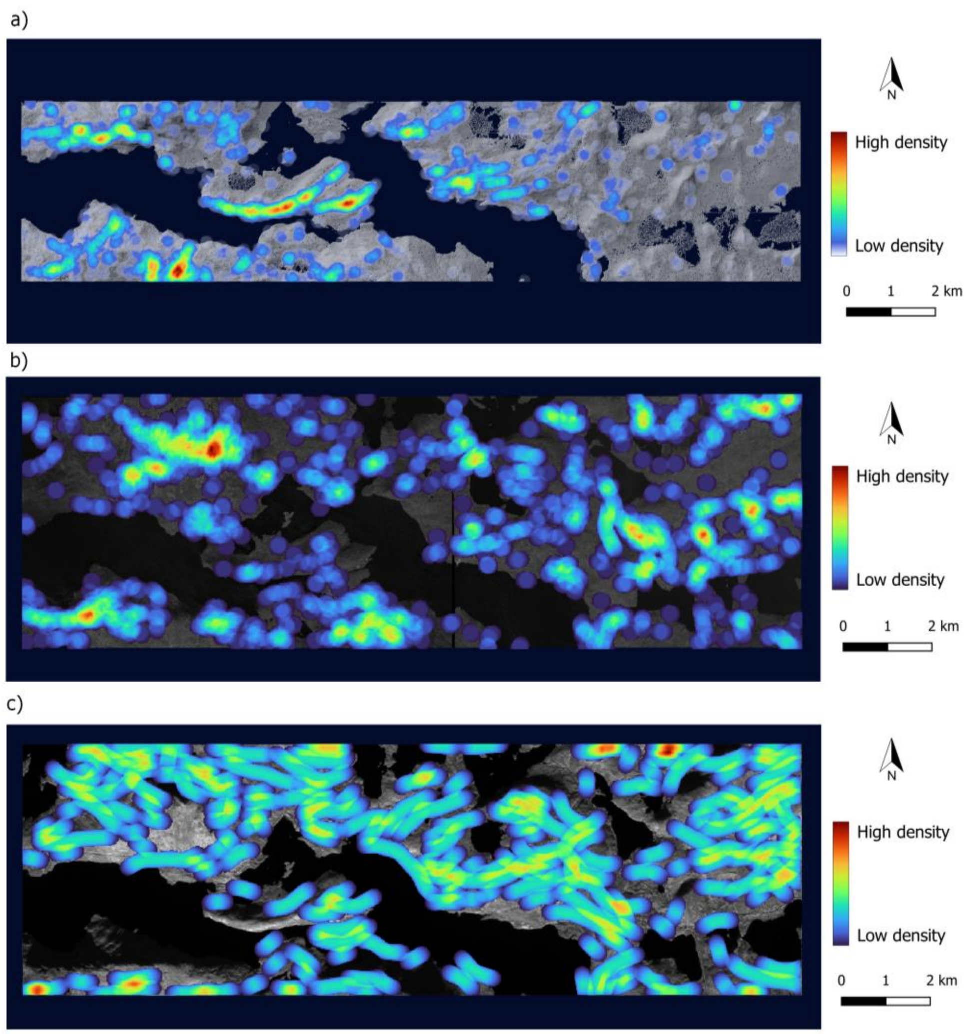

Figure 5. Density maps for lineament extraction. a) Density map for DTM hillshade. b) Density map for WV3 band 7. c) Density map for Sentinel 2 band 8.

4.3 Line bearing

The main direction of the lineaments for the DTM hillshade is ENE – WSW, and the second more expressive orientation has a similar direction (ENE – WSW). The less expressive orientation among these lineaments is SW-NW. For WV3 lineaments the main orientation is E-W, followed by ENE-WSW orientation. The smaller population of lineament corresponds to NNE-SSW (Figure 6 a). The Sentinel 2 and WV3 had similar results concerning the main orientation (E-W), followed by a ENE-WSW trend (Figure 6 b), while the less expressive orientation for Sentinel 2, was SSE-NNW (Figure 6 c). Analysing the results, it is noticeable that the lineaments have an orientation pattern for E-W, ENE-WSW population in line with the results presented by Cardoso-Fernandes et al [13]. The results also show us a smaller orientation pattern corresponding to a N-S, NNE-SSW population, also highlighted by the same authors, that could match potential emplacement structures for Caledonian pegmatites. Comparing the results with the tectonic lineament map of Norway[23], the main orientation of the lineaments doesn't match. For Gabrielsen et al., [23], the main population of the lineaments in northern Norway are oriented according to WNW-ESE, and NW-SE directions. On the other hand, the author points out that the N-S, and NNE-SSW populations occur in lower density in the north, in accordance with the results of this research. The difference in the spatial resolution of the data used may make the difference between the results of this research and Gabrielsen et al.,[23]. While Gabrielsen et al., [23] used Landsat images with 30 m of GSD, the lowest spatial resolution data used in this research were Sentinel 2 images with 10 m of GSD. Nonetheless, the same author[23] highlighted a higher density of E-W trending faults in Northern Norway, probably associated with a later extension and collapse of the Caledonian orogeny, compatible with the major trends observed in WV3 and Sentinel-2 data.

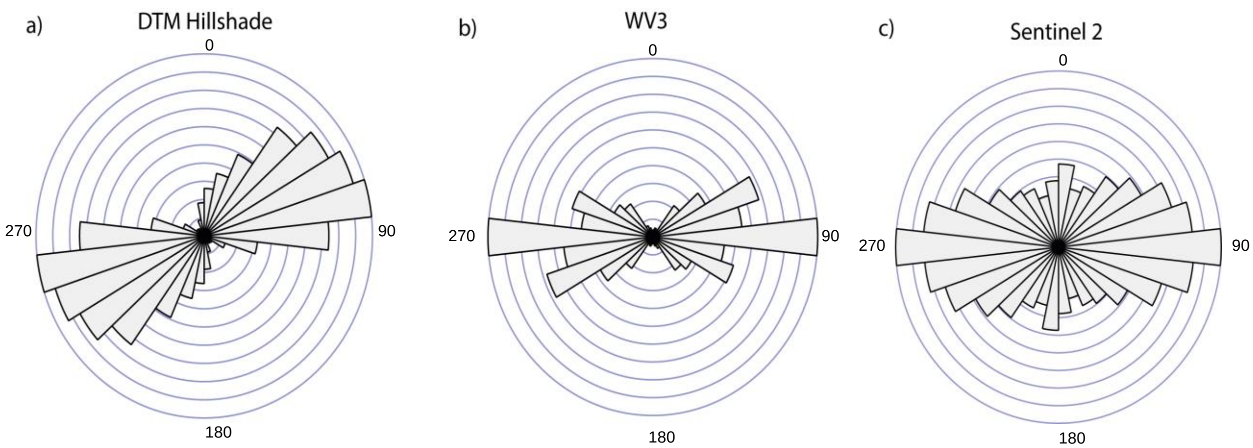

Figure 6. Number of lineaments according to the length and occupational percentage for the automatically extracted. a) DTM hillshade. b) WV3. c) Sentinel 2.

5. CONCLUSIONS

This research explores data at different spatial resolutions to investigate the impact that spatial resolution has on the results of automated lineament extraction. The results reveal a relationship between spatial resolution and the number of extracted lineaments. Higher spatial resolution data led to the identification of more lineaments. Additionally, a correlation between spatial resolution and the length of extracted lineaments was observed. Greater resolution corresponded to narrower ranges of minimum and maximum lineament lengths. Regarding lineament orientation, the findings display a prevailing pattern for E-W and ENE-WSW orientations, while the N-S and NNE-SSW orientations exhibit lower frequencies. However, the latter could match potential emplacement structures for Caledonian pegmatites. In summary, the results indicate significant potential for utilizing high-resolution imagery in automated lineament extraction. In the future, these outcomes could be integrated with other products generated through high-resolution image processing, such as subpixel classification methods. This integration could aid in identifying anomalies indicative of potential points of interest for exploration. The findings highlight that very high-resolution images hold significant potential for extracting lineaments, which in turn can aid in identifying mineral deposits and neotectonic activity. These discoveries can be combined with other remote sensing techniques to amplify the capabilities of remote sensing for mineral exploration.

ACKNOWLEDGMENTS

This study is funded by European Union's Horizon 2020 innovation program under grant agreement No 869274, project GREENPEG: New Exploration Tools for European Pegmatite Green-Tech Resources. The work was also supported by Portuguese National Funds through the FCT project UIDB/04683/2020 - ICT (Institute of Earth Sciences). Douglas Santos was financially supported by Portuguese national funds through FCT (Grant: UI/BD/154412/2023).

REFERENCES

[1] Fan, J. and Ni, C., "Comparative Studies on the Extraction of Lineaments and Its Variability Based on an Improved Line Segment Tracking Method—Taking the Gaosong Ore Field in the Gejiu Gejiu Tin Ore Deposit as an Example," Applied Sciences (Switzerland) **13**(3) (2023).

[2] Das, S., Pardeshi, S., Kulkarni, P. and Doke, A., "Extraction of lineaments from different azimuth angles using geospatial techniques: a case study of Pravara basin, Maharashtra, India," Arabian Journal of Geosciences **11** (2018).

[3] Al-Mokredi, M. S., Guangdao, H. and Al Bassam, B. F., "Using Remote Sensing Data to Delineate the Lineaments for Hydrothermal Mineral Prediction in Heqing Area, Northwest Yunnan Province, China," Journal of China University of Geosciences **18**(2), 142–147 (2007).

[4] Koike, K., Nagano, S. and Ohmi, M., "Lineament analysis of satellite images using a Segment Tracing Algorithm (STA)," Comput Geosci **21**(9), 1091–1104 (1995).

[5] Adiri, Z., El Harti, A., Jellouli, A., Lhissou, R., Maacha, L., Azmi, M., Zouhair, M. and Bachaoui, E. M., "Comparison of Landsat-8, ASTER and Sentinel 1 satellite remote sensing data in automatic lineaments extraction: A case study of Sidi Flah-Bouskour inlier, Moroccan Anti Atlas," Advances in Space Research **60**(11), 2355–2367 (2017).

[6] İkramBoutırame AhmedAkhssas, AhmedManar, A., "Geological structures mapping using aeromagnetic prospecting and remote sensing data in the karstic massif of Beni Mellal Atlas, Morocco," Journal **160**(160), 213–229 (2019).

[7] Cardoso-Fernandes, J., Teodoro, A. C., Lima, A., Menuge, J., Brönner, M. and Steiner, R., "Sentinel-1 and ALOS data for lineament extraction: a comparative study," Proc.SPIE **12268**, 122680X (2022).

[8] Villalta Echeverria, M. D., Viña Ortega, A. G., Larreta, E., Romero Crespo, P. and Mulas, M., "Lineament Extraction from Digital Terrain Derivate Model: A Case Study in the Girón–Santa Isabel Basin, South Ecuador," Remote Sens (Basel) **14**(21) (2022).

[9] Al-Dossary, S. and Marfurt, K. J., "Lineament-preserving filtering," Geophysics **72**(1), P1–P8 (2006).

[10] Tözün, K. A. and Özyavaş, A., "Automatic detection of geological lineaments in central Turkey based on test image analysis using satellite data," Advances in Space Research **69**(9), 3283–3300 (2022).

[11] Müller, A., Romer, R. L., Augland, L. E., Zhou, H., Rosing-Schow, N., Spratt, J. and Husdal, T., "Two-stage regional rare-element pegmatite formation at Tysfjord, Norway: implications for the timing of late Svecofennian and late Caledonian high-temperature events," International Journal of Earth Sciences **111**, 987–1007 (2022).

[12] Rykkelid, E. and Andresen, A., "Late Caledonian extension in the Ofoten area, northern Norway," Tectonophysics **231**(1), 157–169 (1994).

[13] Cardoso-Fernandes, J., Teodoro, A. C. M., Campos de Lima, A. M., Menuge, J., Brönner, M. and Steiner, R., "Sentinel-1 and ALOS data for lineament extraction: a comparative study," 38 (2022).

[14] Chavez Jr, P., "Image-Based Atmospheric Corrections - Revisited and Improved," Photogramm Eng Remote Sensing **62**, 1025–1036 (1996).

[15] Pradhan, B., Ahmed, A. A., Chakraborty, S., Alamri, A. and Lee, C.-W., "Orthorectification of WorldView-3 Satellite Image Using Airborne Laser Scanning Data," J Sens **2021** (2021).

[16] El-Desoky, H. M., Tende, A. W., Abdel-Rahman, A. M., Ene, A., Awad, H. A., Fahmy, W., El-Awny, H. and Zakaly, H. M. H., "Hydrothermal Alteration Mapping Using Landsat 8 and ASTER Data and Geochemical Characteristics of Precambrian Rocks in the Egyptian Shield: A Case Study from Abu Ghalaga, Southeastern Desert, Egypt," Remote Sens (Basel) **14**(14) (2022).

[17] Tripp, G. I. and Vearncombe, J. R., "Fault/fracture density and mineralization: a contouring method for targeting in gold exploration," J Struct Geol **26**(6), 1087–1108 (2004).

[18] Pradesh, A., "Lineament Extraction and Hot Spring Potential zones Demarcation in and around Tawang ," (2011).

[19] Javhar, A., Chen, X., Bao, A., Jamshed, A., Yunus, M., Jovid, A. and Latipa, T., "Comparison of multi-resolution optical Landsat-8, Sentinel-2 and radar Sentinel-1 data for automatic lineament extraction: A case study of Alichur area, SE Pamir," Remote Sens (Basel) **11**(7), 1–29 (2019).

[20] Algouti, A., Algouti, A. and Farah, A., "Mapping and analysis of structural lineaments using SRTM radar data and Landsat 8-OLI images in Telouet-Tighza area , Marrakech High Atlas - Morocco .," Res Sq, 1–21 (2022).

[21] Hashim, M., Ahmad, S., Johari, M. A. M. and Pour, A. B., "Automatic lineament extraction in a heavily vegetated region using Landsat Enhanced Thematic Mapper (ETM+) imagery," Advances in Space Research **51**(5), 874–890 (2013).

[22] Mostafa, M. E. and Qari, M. Y. H. T., "An exact technique of counting lineaments," Eng Geol **39**(1), 5–15 (1995).

[23] Gabrielsen, R. H., Braathen, A., Dehis, J. and Roberts, D., "Tectonic lineaments of Norway," Norsk Geologisk Tidsskrift **82**(3), 153–174 (2002).